JACS
JOURNAL OF THE AMERICAN CHEMICAL SOCIETY
Article
pubs.acs.org/JACS

Hollow Cobalt-Based Bimetallic Sulfide Polyhedra for Efficient All-pH-Value Electrochemical and Photocatalytic Hydrogen Evolution

Zhen-Feng Huang,[†,‡] Jiajia Song,[†,‡] Ke Li,[†,‡] Muhammad Tahir,[†,‡,§] Yu-Tong Wang,[†,‡] Lun Pan,[†,‡] Li Wang,[†,‡] Xiangwen Zhang,[†,‡] and Ji-Jun Zou*[,†,‡]

[†]Key Laboratory for Green Chemical Technology of the Ministry of Education, School of Chemical Engineering and Technology, Tianjin University, Tianjin 300072, China

[‡]Collaborative Innovative Center of Chemical Science and Engineering (Tianjin), Tianjin 300072, China

[§]Department of Physics, The University Of Lahore, Punjab 54600, Pakistan

Supporting Information

ABSTRACT: The development of highly active, universal, and stable inexpensive electrocatalysts/cocatalysts for hydrogen evolution reaction (HER) by morphology and structure modulations remains a great challenge. Herein, a simple self-template strategy was developed to synthesize hollow Co-based bimetallic sulfide ($M_xCo_{3-x}S_4$, M = Zn, Ni, and Cu) polyhedra with superior HER activity and stability. Homogenous bimetallic metal−organic frameworks are transformed to hollow bimetallic sulfides by solvothermal sulfidation and thermal annealing. Electrochemical measurements and density functional theory computations show that the combination of hollow structure and homoincorporation of a second metal significantly enhances the HER activity of Co_3S_4. Specifically, the homogeneous doping in Co_3S_4 lattice optimizes the Gibbs free energy for H* adsorption and improves the electrical conductivity. Impressively, hollow $Zn_{0.30}Co_{2.70}S_4$ exhibits electrocatalytic HER activity better than most of the reported nobel-metal-free electrocatalysts over a wide pH range, with overpotentials of 80, 90, and 85 mV at 10 mA cm^{-2} and 129, 144, and 136 mV at 100 mA cm^{-2} in 0.5 M H_2SO_4, 0.1 M phosphate buffer, and 1 M KOH, respectively. It also exhibits photocatalytic HER activity comparable to that of Pt cocatalyst when working with organic photosensitizer (Eosin Y) or semiconductors (TiO_2 and C_3N_4). Furthermore, this catalyst shows excellent stability in the electrochemical and photocatalytic reactions. The strategy developed here, i.e., homogeneous doping and self-templated hollow structure, provides a way to synthesize transition metal sulfides for catalysis and energy conversion.

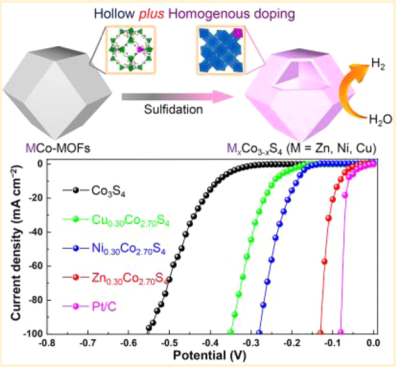

1. INTRODUCTION

Hydrogen, as a clean renewable energy source of fuel, is one of the most promising energy carriers for replacing traditional fossil fuels. Water electrolysis driven by renewable-resource-derived electricity and water splitting driven by solar-energy photocatalysis are promising pathways for sustainable hydrogen production.[1] Hydrogen evolution reaction (HER) requires high-performance electrocatalyst/cocatalyst to promote the sluggish kinetics. Pt is the most active HER catalyst, but the concerns related to its higher cost and rarity are big hurdles for practical application.[1c,d,f] Therefore, numerous efforts have been devoted to exploring stable and noble-metal-free HER catalyst with good efficiency. In this regard, transition metal sulfides have been recently suggested as promising catalyst for HER,[2] inspired by the structure/composition of nitrogenase and hydrogenase.[3] However, their activity is far from satisfactory compared with that of noble Pt catalyst, and most of them work only in acidic media. Enhancing the electrical conductivity and increasing the number of exposed surface active sites are effective ways to improve the activity.[4] Specifically, homobimetallic sulfides, different from surface doping and heterojunction at surface/interface, are believed to manipulate the inherent electronic and/or surface structures of the host material toward better activity more effectively.[2c,5] Moreover, very recent work shows that doping metal sulfides with secondary metal ions may produce catalyst that can work in alkaline and neutral medium.[6] However, such homogeneous composition is hard to achieve mainly because of the difficulty in preparing homobimetallic precursors.

Porous/hollow structures have attracted much attention in catalysis because of the intriguing features such as large surface area, low density, kinetically favorable open structure, and surface permeability,[7] but fabrication of hollow nanomaterials with delicately controlled composition and morphology is still a challenge. Hollow micro-/nanostructures can be produced using a template method including hard, sacrificial, and soft templates.[8] Specifically, metal−organic frameworks (MOFs) are a promising sacrificial template or self-template to construct hollow or porous structures.[9] Moreover, the good compatibility

Received: November 16, 2015
Published: January 16, 2016

DOI: 10.1021/jacs.5b11986
J. Am. Chem. Soc. 2016, 138, 1359−1365

of organic frameworks with various metal ions makes it easy to synthesize homogeneous multimetallic MOFs. With them as precursor, it is possible to fabricate homogeneous multimetallic materials with controllable composition.

Here we report a generalized method to synthesize hollow bimetallic sulfides ($M_xCo_{3-x}S_4$) with homogeneous composition (Scheme 1). Homogenous bimetallic MOFs are used as

Scheme 1. Schematic Illustration of Fabrication of Hollow Co-Based Bimetallic Sulfides

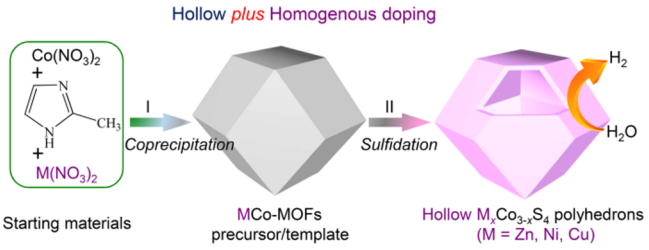

self-templates and precursors to synthesize bimetallic sulfides via solvothermal sulfidation reaction and thermal annealing. Importantly, we also report that $M_xCo_{3-x}S_4$ especially $Zn_{0.30}Co_{2.70}S_4$ shows excellent electrochemical HER activity better than that of most of the reported non-noble-metal catalysts over a wide pH range (pH 0−14). Moreover, the material also demonstrates excellent photocatalytic HER activity that is comparable to that of Pt. Note that pristine Co_3S_4 is not a good HER catalyst compared with other sulfides. However, the activity is improved to a superior level because of the synergetic effect between homogeneous incorporation of second metals in the lattice and formation of hollow structure.

2. EXPERIMENTAL SECTION

2.1. Materials. Eosin Y (EY), $Co(NO_3)_2{\cdot}6H_2O$, $Zn(NO_3)_2{\cdot}6H_2O$, $Ni(NO_3)_2{\cdot}6H_2O$, $Cu(NO_3)_2{\cdot}3H_2O$, and thioacetamide (TAA) were obtained from J&K Chemical. Methanol, absolute ethanol, and isopropanol were purchased from Tianjin Guangfu Fine Chemical Research Institute. Nafion solution (5 wt %) and 2-methylimidazole were obtained from Sigma-Aldrich. All the chemicals are reagent-grade and used as received. High-purity water (18.25 MΩ·cm) supplied by a UP Water Purification System was used in all the experiments.

2.2. Synthesis of Hollow $M_xCo_{3-x}S_4$ Polyhedra. The synthesis of MCo-MOFs is similar to literatures that can be seen in the Supporting Information.[9d,e] Then, 80 mg of MCo-MOFs was redispersed into 40 mL of ethanol, followed by the addition of 0.12 g of TAA. Thereafter, the mixture was transferred into a Teflon-lined stainless-steel autoclave and heated at 120 °C for 4 h. The formed $M_xCo_{3-x}S_4$ hollow polyhedra were centrifuged and washed with ethanol for several times. Finally, they were annealed under N_2 atmosphere at 350 °C for 2 h.

2.3. Characterization. X-ray diffraction (XRD) was carried out with a Bruker D8 Focus operating at 40 kV and 40 mA equipped with a nickel-filtered Cu Kα radiation (λ = 1.54056 Å). Field-emission scanning electron microscopy (FE-SEM) images were obtained using a Hitachi S-4800 SEM. TEM images and corresponding electron energy loss spectroscopy elemental mapping data (EELS) were obtained using a JEM-2100F transmission electron microscope at 200 kV. Element composition was analyzed using a VISTA-MPX EL02115765 inductive coupled plasma atomic emission spectrometer (ICP AES). BET surface area was determined using N_2 adsorption/desorption isotherm measurements at −196 °C on a Micrometrics TriStar 3000 equipment. UV−vis diffuse reflectance spectra (UV−vis DRS) were recorded with a Hitachi U-3010 spectrometer using $BaSO_4$ as the reference. X-ray photoelectron spectroscopy (XPS) data were obtained on a PHI-1600 instrument equipped with Al Kα radiation.

2.4. Electrocatalytic HER. All the electrochemical measurements were conducted using an IVIUMSTAT working station (Ivium Technologies BV, Netherlands) in a typical three-electrode setup with an electrolyte solution, a graphite rod as the counter electrode, and a saturated calomel electrode (SCE) as the reference electrode. The reference electrode is previously calibrated in H_2 saturated electrolyte with respect to an in situ reverse hydrogen electrode (RHE) by using platinum wires as working electrodes, which yields the relation $E(RHE) = E(SCE) + 0.279$ V in 0.5 M H_2SO_4 solution.[1f,2c] A glassy-carbon electrode with a diameter of 3 mm covered by a thin catalyst film was used as the working electrode. Typically, 4 mg of catalyst was suspended in 1 mL of water−isopropanol solution with volume ratio of 3:1 with 50 μL of Nafion solution to form a homogeneous ink assisted by ultrasound for 3 h. Then, 5 μL of the ink was spread onto the surface of glassy-ccarbon electrode (loading 0.285 mg cm^{-2}) by a micropipette and dried under room temperature. Then, 3 μL of 5 wt % Nafion solution was drop-cast on top to protect the film. Electrochemical measurements were conducted in 0.5 M H_2SO_4, 0.1 M phosphate buffer, and 1 M KOH, respectively. For linear sweep voltammetry (LSV) measurements, the scan rate was set to 5 mV s^{-1}. The polarization curves were plotted as overpotential (η) versus log current (log J) to get Tafel plots for assessing the HER kinetics. The Tafel slope (b) was obtained by fitting the linear portion of Tafel plots to the Tafel equation ($\eta = b \log (J) + a$). Primary tests showed that data with and without iR compensation are identical (Figure S1), so all data were reported without iR compensation.[1g,2c,g]

2.5. Photocatalytic HER. The photocatalytic hydrogen production experiments were carried out in a closed 50 mL flask vertically irradiated by a 300 W high-pressure xenon lamp (PLS-SXE300UV, Beijing Trusttech. Co., Ltd.). UV light (220−400 nm, 36.5 mW cm^{-2} at 365 nm) was separated by a UV−ref optical filter. Visible light (>400 nm, 43.0 mW cm^{-2} at 420 nm) was separated by UV−IR−cut filter. For EY-sensitized reactions under visible light, 1.0 mg of sulfides or Pt/C (20 wt %) and 3.5 mg of EY dye were stirred in 20 mL of TEOA-H_2O solution (5%, v/v). For semiconductor catalytic reactions, 0.2 mg of sulfides or in situ photodeposited Pt,[1c,d] 20 mg of TiO_2 (C_3N_4), 20 mL of CH_3OH(TEOA)-H_2O solution (5%, v/v), and UV(visible) light irradiation were used. Prior to irradiation, the reactor was deaerated by bubbling Ar for 30 min to remove air. The amount of evolved H_2 was monitored by a gas chromatograph (Bruker, GC-450, TCD, Ar carrier). TiO_2 was from Degussa:Hulls Corporation. C_3N_4 was synthesized by calcining urea at 600 °C for 4 h according to literature.[7d]

2.6. Density Functional Theory Calculations. The electronic structures and adsorption free energy were computed by Vienna ab initio Simulation package (VASP) using spin-polarized density functional with the Hubbard model (DFT+U).[10a,b] The projector augmented wave (PAW) model with Perdew−Burke−Ernzerhof (PBE) function was employed to describe the interactions between core and electrons, and the value of the correlation energy (U) was fixed at 5.9, 7.5, 6.4, and 4.0 eV for the 3d orbits of Co, Zn, Ni, and Cu, respectively.[10c,d] An energy cutoff of 550 eV was used for the plane-wave expansion of the electronic wave function. The Brillouin zones of all systems were sampled with gamma-point centered Monkhorst−Pack grids. A 3 × 3 × 3 and 3 × 3 × 1 Monkhorst Pack k-point setup were used for bulk and slab geometry optimization, while 9 × 9 × 9 for the density of states and electronic band structure. The force and energy convergence criterion were set to 0.02 eV $Å^{-1}$ and 10^{-5} eV, respectively. Molecular model building details and free-energy calculations are given in the Supporting Information.

3. RESULTS AND DISCUSSION

3.1. Formation of Homogenous Bimetallic MOFs. Bimetallic MOFs (designated as MCo-MOFs, M = Zn, Ni, and Cu) were synthesized via room-temperature coprecipitation reaction of $Co(NO_3)_2$ and $M(NO_3)_2$ mixtures with 2-methylimidazole in methanol. (For details, see the experimental section in the Supporting Information.) Theoretically, M^{2+} can be homogeneously introduced in the Co-MOF framework by

DOI: 10.1021/jacs.5b11986
J. Am. Chem. Soc. 2016, 138, 1359−1365

substituting Co^{2+} sites because of their similar ionic radius and electronegativity (Figure 1a and Tables S1 and S2).[9d,e] XRD

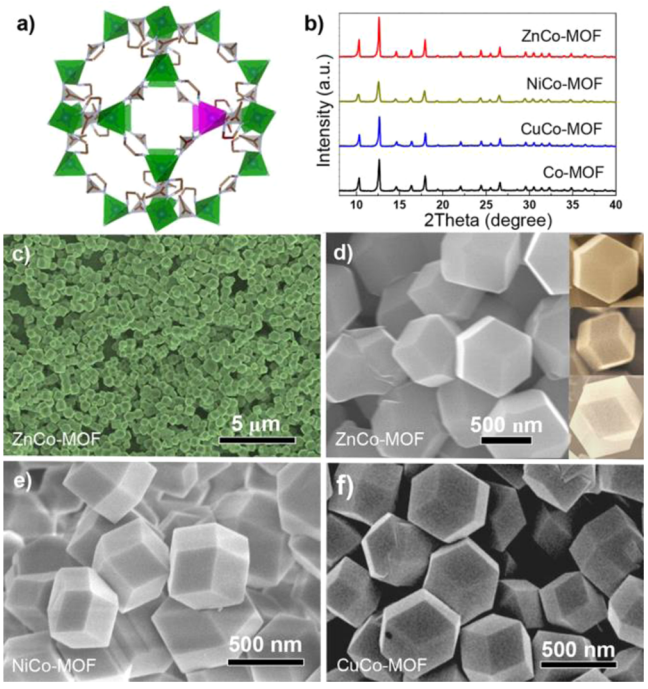

Figure 1. (a) Unit of bimetallic MCo-MOF. Green color indicates the sites of Co atom, whereas pink shows the sites of substitutional M atom. (b) XRD patterns of $M_{0.30}Co_{2.70}$-MOF and Co-MOF. (c–f) SEM images of $M_{0.30}Co_{2.70}$-MOF (M = Zn, Ni, and Cu).

patterns of all MCo-MOFs samples exhibit strong diffraction peaks at identical positions similar to Co-MOF (Figures 1b and S2). The atomic ratios of M/Co detected by ICP in as-synthesized samples are very close to those in the starting materials (Table S3), indicating the effective coprecipitation of all metal ions with 2-methylimidazole. Additionally, the color of both ZnCo-MOFs (even at molar ratio of $Zn^{2+}/Co^{2+} = 1$) and Co-MOF are purple, very different from the white color of Zn-MOFs (Figure S3). This phenomenon visually confirms that Zn ions are incorporated in the frame of Co-MOF instead of separate Zn-MOF phase. SEM images (Figure 1c–f) show that the as-synthesized MOFs are highly uniform polyhedra with size of ca. 600 nm. Different view positions of a single particle (Figure 1d, inset) reveal that it has a well-defined rhombic dodecahedral morphology.

3.2. Formation of Homogenous Bimetallic Cobalt Sulfides. The formation of homobimetallic MOF provides a chance to fabricate homobimetallic sulfides. In detail, the bimetallic sulfides can be produced by in situ topotactic transformation of MOFs in TAA solution, as follows:

$$CH_3CSNH_2 + C_2H_5OH \rightarrow CH_3(NH_2)C(OC_2H_5)-SH \quad (1)$$

$$CH_3(NH_2)C(OC_2H_5)-SH + C_2H_5OH \rightarrow CH_3(NH_2)C(OC_2H_5)_2 + H_2S \quad (2)$$

$$4H_2S + M_xCo_{3-x}(C_4H_5N_2)_8 \rightarrow M_xCo_{3-x}S_4 + 8C_4H_6N_2 \quad (3)$$

Upon further thermal annealing in N_2 atmosphere, the rhombic dodecahedral morphology of MOF precursors is well-maintained, but the crystallinity is greatly improved (Figures 2a, S4, and S5).

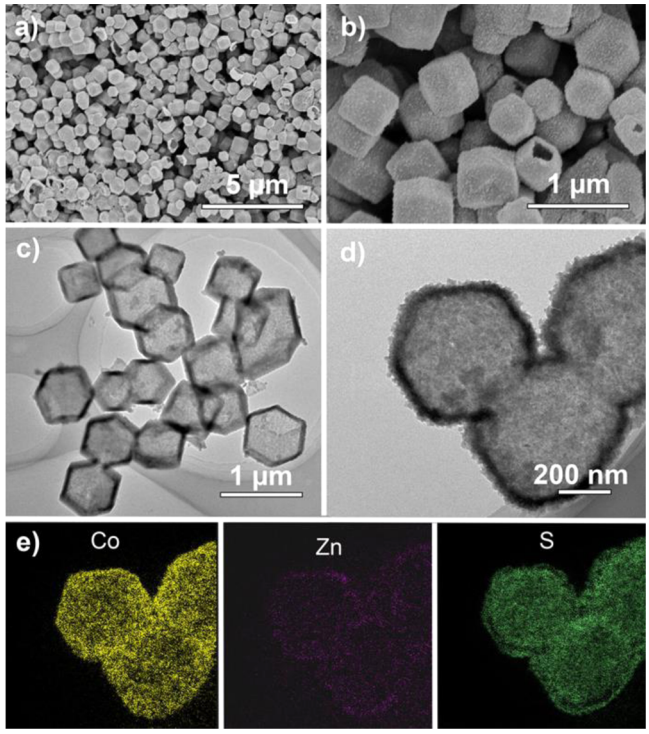

Figure 2. (a and b) SEM and (c and d) TEM images of $Zn_{0.30}Co_{2.70}S_4$, and (e) EELS element mapping of zone shown in d.

The formation of a hollow structure can be discerned unambiguously from some cracked particles (Figure 2b). TEM provides further insight into the hollow interior and detailed structure (Figure 2c). The well-defined inner cavities inside the uniform polyhedra are clearly elucidated by the sharp contrast between the center and the edge. The shell has a thickness of ca. 30–50 nm and is robust enough to endure the sulfidation reaction and subsequent thermal annealing. High-resolution TEM images (Figures 2d and S5b) reveal that the shell is composed of nanoparticles of ca. 20 nm. The hollow polyhedrals afford high BET specific surface area (125, 109, 121, and 147 m^2g^{-1}) and large pore volume (0.91, 0.81, 0.87, and 1.17 cm^3g^{-1} for $Zn_{0.30}Co_{2.70}S_4$, $Ni_{0.30}Co_{2.70}S_4$, $Cu_{0.30}Co_{2.70}S_4$, and Co_3S_4, respectively).

XRD (Figure 3a) shows that the sulfides can be indexed as cubic Co_3S_4 (Powder Diffraction File No. 47-1738, Joint Committee on Powder Diffraction Standards, [1969]). Particularly, the incorporation of second metals (Zn, Cu, and Ni) does not affect the spinel structure, and there is no new peak originating from other metal sulfides, indicating the homogeneous incorporation of metal ions into the lattice of Co_3S_4 by taking the sites of Co ions (Figure 3b,c). Moreover, the peaks of doped Co_3S_4 do not show any shift compared to those of pristine Co_3S_4, suggesting the doping almost does not influence the cell parameters because of the very similar ionic radius of guest and host metal ions. The uniform distribution of metal and S species is also confirmed by EELS element mapping (Figure 2e), and the M/Co ratio in sulfides is very close to that of bimetallic MCo-MOF precursors (Table S3). XPS analysis also excludes the existence of carbon and nitrogen residues in the sulfides (Figure S6).

DOI: 10.1021/jacs.5b11986
J. Am. Chem. Soc. 2016, 138, 1359–1365

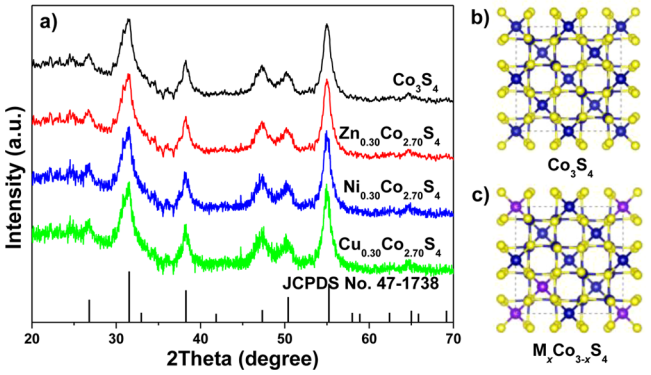

Figure 3. (a) Powder XRD patterns and (b and c) cell units of Co_3S_4 and $M_xCo_{3-x}S_4$. Blue, yellow, and purple balls represent Co, S, and M atoms, respectively; M atom dopant is introduced to substitute Co^{2+}.

Time-dependent experiments were carried out to monitor the formation process of hollow sulfides (Figure 4a). At the beginning of sulfidation procedure, S^{2-} ions released from TAA upon hydrolyzation quickly react with metal ions on MOFs surface to form a thin layer of sulfides, which acts as a physical barrier to prevent the direct contact and chemical reaction between outside sulfide ions and inner metal ions. EELS element mapping (Figure 4b) confirms the formation of MOF@metal sufide core/shell structure. Then, metal and/or sulfide ions have to diffuse through this newly formed sulfide layer to continue the sulfidation reaction. Because the ionic radius of metal ions (72−74 pm) is significantly smaller than that of S^{2-} ions (184 pm) (Table S1), the outward diffusion of metal ions is much easier than the inward diffusion of S^{2-} ions. Therefore, the inner organic framwork is gradually dissolved, and the released metal ions penetrate the preformed shell to react with S^{2-} ions on the outer surface, which finally produces a hollow void inside the shell. In this case, the MOF precusors serve as a self-template to produce hollow polyhedra morphology. Importantly, this strategy can be extended to fabricate other hollow binary and monometal sulfides with tunable compostion using corresponding MOF as the precursor (Figures 3a, 4c,d, S4, and S7b and Table S3).

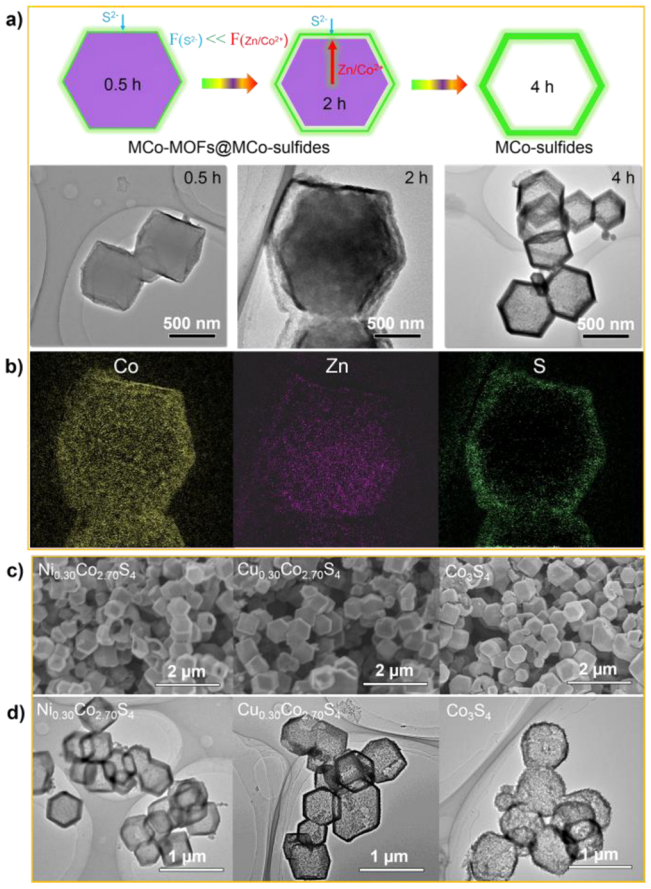

Figure 4. (a) Time-dependent formation of hollow $Zn_{0.30}Co_{2.70}S_4$ polyhedra. (b) EELS element mapping of ZnCo-MOF after 2 h of sulfidation reaction. (c and d) SEM and TEM images of $Ni_{0.30}Co_{2.70}S_4$, $Cu_{0.30}Co_{2.70}S_4$, and Co_3S_4, respectively.

3.3. Superior Electrocatalytic Performance in Acidic Media. The homogeneous incorporation of second metal in Co_3S_4, different from the surface doping/heterojunction,[2c,5a,11a] provides a good platform to investigate the relationship between activity and composition. The electrocatalytic HER activity of $M_xCo_{3-x}S_4$ in acidic media (pH 0) was evaluated with commercially available Pt/C catalyst (20 wt %) as reference. The bimetallic sulfides show obviously enhanced performance compared with Co_3S_4, with the overpotential at 10 mA cm^{-2} (η_{10}) decreasing from 380 mV for pristine Co_3S_4 to 243 mV for $Cu_{0.30}Co_{2.70}S_4$, 186 mV for $Ni_{0.30}Co_{2.70}S_4$, and 80 mV for $Zn_{0.30}Co_{2.70}S_4$, (Figure 5a). For $Zn_xCo_{3-x}S_4$ with a different Zn/Co molar ratio, an optimal HER catalytic activity presents when x = 0.3, with the lowest onset overpotential of 35 mV (Figure S8), and a rapid cathodic current increases at higher bias along with vigorous evolution of H_2 bubbles from the electrode surface (Video S1). $Zn_{0.30}Co_{2.70}S_4$ electrode also produces a catalytic current density of 100 mA cm^{-2} with a low overpotential of 129 mV. By plotting overpotential (η) against log current (log J), the kinetic parameters of HER were calculated. The linear part of Tafel plots (Figure 5b) reveals Tafel slopes of ~30.4, ~ 85.3, and ~47.5 mV dec^{-1} for Pt/C, Co_3S_4, and $Zn_{0.30}Co_{2.70}S_4$, respectively. This suggests that hydrogen evolution over $Zn_{0.30}Co_{2.70}S_4$ proceeds via the Volmer−Heyrovsky mechanism and that the electrochemical

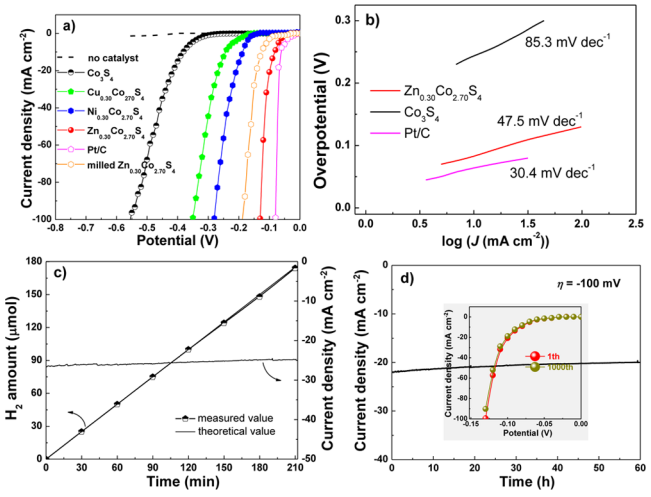

Figure 5. (a) Polarization data of $M_xCo_{3-x}S_4$, Co_3S_4, and Pt/C electrodes in 0.5 M H_2SO_4. (b) Tafel plots. (c) Amount of H_2 production over $Zn_{0.30}Co_{2.70}S_4$ at a current density of ca. 25 mA cm^{-2}. (d) Time-dependent current density curve of HER over $Zn_{0.30}Co_{2.70}S_4$ at η = −100 mV over 60 h (Inset: polarization curve after 1000 cycles).

DOI: 10.1021/jacs.5b11986
J. Am. Chem. Soc. 2016, 138, 1359−1365

desorption step is rate-limiting. By further applying the extrapolation method to the Tafel plots (Figure S9), the exchange current density (J_0) of 0.15 mA cm^{-2} was obtained for $Zn_{0.30}Co_{2.70}S_4$, which is 6 times larger than that of pristine Co_3S_4 (0.025 mA cm^{-2}). It is worth noting that such high catalytic activity, i.e., low overpotential, low Tafel slope, and high exchange current density of hollow $Zn_{0.30}Co_{2.70}S_4$ polyhedra, is much better than most of those for the reported noble-metal-free HER catalysts (with similar catalyst loading) including transition metal sulfides, selenides, phosphides, carbides, and nitrides, and metal-free carbon-based materials (Table S4).

Figure 5c compares the amount of H_2 generated over hollow $Zn_{0.30}Co_{2.70}S_4$ versus theoretically possible H_2 amount that can be evolved from electrochemical HER. $Zn_{0.30}Co_{2.70}S_4$ shows not only a stable HER performance but also a rate (49.7 μmol h^{-1}) very close to the theoretically achievable value. In other words, $Zn_{0.30}Co_{2.70}S_4$ gives about 100% faradaic yield and has excellent stability in electrochemical HER. Actually, it retains the activity and morphology even after 60 h of testing (Figures 5d and S10), with no change in the polarization curve after 1000 cycles (Figures 5d, inset). In contrast, Co_3S_4 shows evidently decreased HER activity after 10 h, with the retention of current density about 75% (Figure S11). Therefore, Zn doping not only enhances HER activity but also significantly promotes the stability of Co_3S_4.

When $Zn_{0.30}Co_{2.70}S_4$ hollow polyhedra are converted into powders by ball milling (Figure S12), the activity is decreased evidently with η_{10} of 125 mV (Figure 5a), indicative of the advantage of hollow structure. Even still, the $Zn_{0.30}Co_{2.70}S_4$ powders still show much better activity than hollow Co_3S_4, $Cu_{0.30}Co_{2.70}S_4$, and $Ni_{0.30}Co_{2.70}S_4$. Furthermore, electrochemical double layer capacitance (Figure S13a) reveals an electrochemical active surface area (ECSA) of bimetallic sulfides (46.9, 43.1, 41.5, and 41.3 mF cm^{-2} for $Zn_{0.30}Co_{2.70}S_4$, milled $Zn_{0.30}Co_{2.70}S_4$, $Ni_{0.30}Co_{2.70}S_4$, and $Cu_{0.30}Co_{2.70}S_4$, respectively) higher than that of Co_3S_4 (32.5 mF cm^{-2}). Note that pure ZnS exhibits negligible HER activity (Figure S7c). Therefore, Co_3S_4 is the major catalyst, and the homogeneous doping of Zn ions contributes to the catalytic performance. It is also noted that the catalyst without thermal annealing has a low activity because of the poor crystallinity (Figure S1).

3.4. Optimized Electronic Structure and H* Adsorption. Nyquist plots (Figure S13b) reveal a dramatically decreased charge transfer resistance (R_{ct}) for bimetallic sulfides (3.7, 10.5, and 25.1 Ω for $Zn_{0.30}Co_{2.70}S_4$, $Ni_{0.30}Co_{2.70}S_4$, and $Cu_{0.30}Co_{2.70}S_4$, respectively, compared to 66.1 Ω for Co_3S_4). Theoretical calculation was further used to verify the enhanced electrical conductivity. As shown in calculated density of states (Figure 6a), the incorporation of Zn^{2+} into Co_3S_4 can narrow the band gap from 0.82 to 0.68 eV. This band gap narrowing leads to the enhanced excitation of charge carriers to the conduction band, which is beneficial for the electrical conductivity and the electrochemical performance.[2b,11b,c] The band gap can be further reduced by introducing other metal ions such as Ni^{2+} and Cu^{2+}. The reduced band gap is attributed to the enhanced hybridization between Co d orbital and S p orbital,[2b] as illustrated by charge density distribution (Figures 6b and S14).

DFT calculations were also carried out to gain further insights into the nature of the catalytic process. The HER can be summarized in a three-state diagram, consisting of an initial H^+ state, an intermediate H* state, and $^1/_2H_2$ as the final

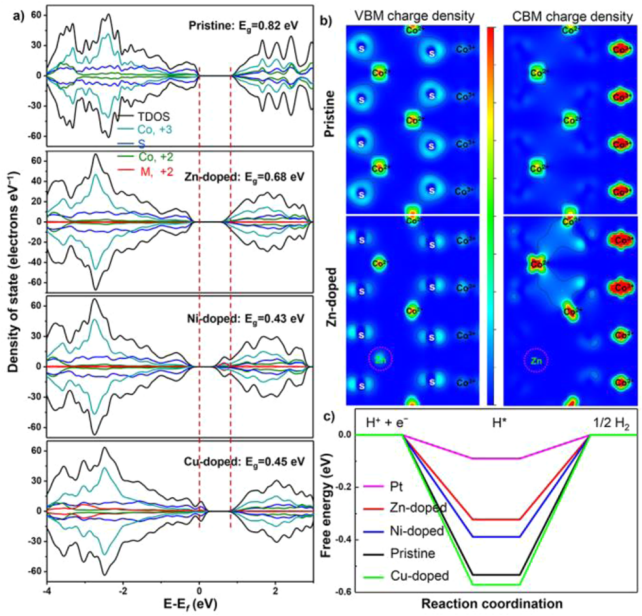

Figure 6. (a) Projected density of states of pristine and Zn-, Ni-, and Cu-doped Co_3S_4. (b) Difference charge density of valence band (left) and conduction band (right) in pristine and Zn-doped Co_3S_4. Red and blue colors represent electron accumulation and electron depletion. (c) Calculated free-energy diagram of HER at equilibrium potential on pristine and Zn-, Ni-, and Cu-doped Co_3S_4.

product (Figure 6c).[12a] A good catalyst for HER should have a moderate free energy for H adsorption (ΔG_H*) to compromise for the reaction barriers of the adsorption and desorption steps.[12a] The $|\Delta G_H^*|$ value of the most efficient catalyst, Pt, is nearly 0.09 eV, which is very close to thermoneutral. Our calculations show that second-metal doping can significantly influence the $|\Delta G_H^*|$ value of Co_3S_4. For instance, the $|\Delta G_H^*|$ value of Zn-doped Co_3S_4 is 0.32 eV, comparable to many active non-noble-metal catalysts.[12] In addition, the $|\Delta G_H^*|$ value of Ni-doped Co_3S_4 is 0.39 eV, also significantly lower than that of Co_3S_4 (0.53 eV). Contrarily, Cu-doped Co_3S_4 shows very strong hydrogen adsorption ($|\Delta G_H^*|$ = 0.57 eV), which counteracts the enhanced electrical conductivity. The collaborative effect of electrical conductivity and hydrogen adsorption explains why Zn-doping has excellent HER activity.

3.5. Universal Electrocatalyst over a Wide pH Range. Until now, most non-noble-metal HER electrocatalysts work well only in acidic medium to catalyze the conversion of H_3O^+, and the HER activities in alkaline and neutral media to catalyze the conversion of H_2O are usually about 2−3 orders of magnitude lower than those in acidic medium.[6a,13] However, many water−alkali and chloro−alkali HER electrolyzers need active and durable catalysts that can work in alkaline medium, and many microbial electrolysis cells typically need electrocatalysts that can function well in neutral medium. As shown in Figures 5a and 7a,b, Co_3S_4 exhibits very similar activity when the pH value changes from 0 to 14, which suggests that Co_3S_4-based material may be a good candidate to work at all pH values. Actually, it is reported that the HER activity of amorphous CoS_x is almost independent of pH value.[6a]

Upon further incorporation of Zn, $Zn_{0.30}Co_{2.70}S_4$ exhibits remarkably improved HER activity both in neutral and alkaline media compared to that of Co_3S_4, affording a current density of 10 mA cm^{-2} at overpotential of 90 and 85 mV, respectively, which is better than most of the reported non-noble-metal

DOI: 10.1021/jacs.5b11986
J. Am. Chem. Soc. 2016, 138, 1359−1365

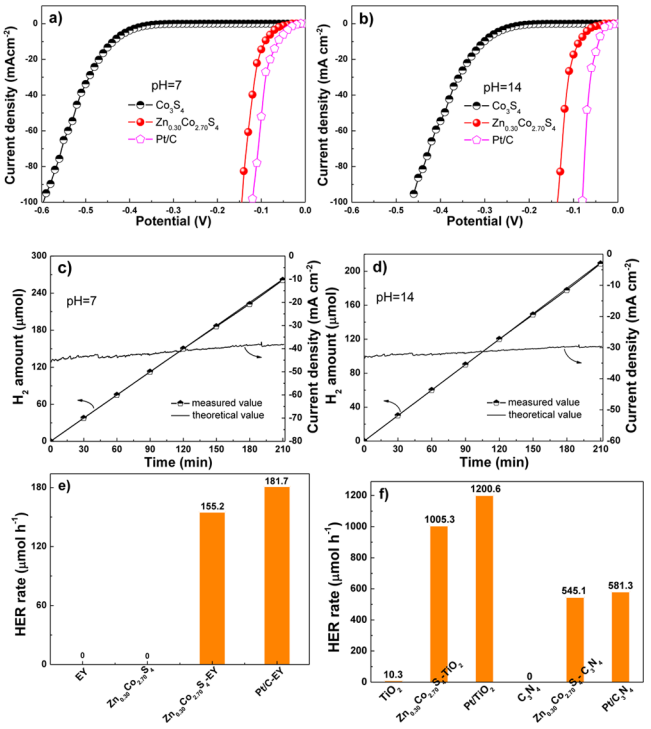

Figure 7. (a and b) Polarization data of $Zn_{0.30}Co_{2.70}S_4$, Co_3S_4 and Pt/C electrodes at pH 7 and 14. (c and d) Electrocatalytic hydrogen production over $Zn_{0.30}Co_{2.70}S_4$ at pH 7 and 14. (e) Photocatalytic HER rate over EY-sensitized $Zn_{0.30}Co_{2.70}S_4$ under visible light. (f) Photocatalytic HER rate over $Zn_{0.30}Co_{2.70}S_4$–TiO_2 under UV light and $Zn_{0.30}Co_{2.70}S_4$–C_3N_4 under visible light.

based HER electrocatalysts (with similar catalyst loading) (Table S4). Additionally, $Zn_{0.30}Co_{2.70}S_4$ shows excellent stability and about 100% faradaic yield in both media (Figure 7c,d). These results clearly indicate that $Zn_{0.30}Co_{2.70}S_4$ is a universal and efficient HER electrocatalyst over a wide pH range (pH 0–14). Recent work also shows that MoS_x doped with Co or Ni ions can be operated in alkaline and neutral media with considerable HER activity and stability.[6] The secondary metal incorporation is very likely to promote the water dissociation that is the first step for HER in alkaline and neutral media.[6a] Then, the optimized H adsorption (ΔG_H* in Figure 6c) by doping facilitates the formation of H_2 from the H intermediates of water dissociation.[13c]

3.6. Excellent Photocatalytic HER Performance. Hollow $Zn_{0.30}Co_{2.70}S_4$ also works very well as cocatalyst in photocatalytic HER. In photocatalysis, dyes and semiconductors can absorb light and generate and transfer electrons to cocatalyst for H_2 evolution (Figure S15). Figure 7e shows a promising H_2 evolution rate of 155.2 μmol h^{-1} over $Zn_{0.30}Co_{2.70}S_4$ when sensitized by Eosin Y dye under visible light, which is comparable to the activity of Pt/C (188.7 μmol h^{-1}). Furthermore, the H_2 evolution rate is very stable during a long-term test (Figure S16). TiO_2 and C_3N_4 are promising UV- and visible-response semiconductors,[1h,i,7d] respectively (Figure S17). When combined with them, $Zn_{0.30}Co_{2.70}S_4$ shows HER activity very close to that of Pt (Figure 7f).

4. CONCLUSIONS

A general MOF self-templated method to synthesize hollow bimetallic sulfide ($M_xCo_{3-x}S_4$) polyhedra has been established. The second metal ions are homogeneously dispersed in the lattice of Co_3S_4 because of the homogeneous composition of MOF precursor. The incorporation of second metal and the formation of hollow structure improve the catalytic active sites optimize the electrical conductivity and hydrogen adsorption of Co_3S_4. The bimetallic sulfides exhibit significantly improved electrochemical and photocatalytic HER activities compared with those of pristine Co_3S_4. Particularly, $Zn_{0.30}Co_{2.70}S_4$ shows electrochemical HER activity over a wide pH range (pH 0–14) better than most of those of reported noble-metal-free catalysts and photocatalytic HER activity comparable to that of Pt. The strategy developed here, i.e., homogeneous doping and self-templated hollow structure, provides a way to synthesize transition metal sulfides for catalysis and energy conversion.

■ ASSOCIATED CONTENT

Supporting Information

The Supporting Information is available free of charge on the ACS Publications website at DOI: 10.1021/jacs.5b11986.

Detailed experimental and computation procedures, results of characterizations. (PDF)

Video showing vigorous evolution of H_2 bubbles from the electrode surface at various overpotentials. (AVI

■ AUTHOR INFORMATION

Corresponding Author

*E-mail: jj_zou@tju.edu.cn.

Notes

The authors declare no competing financial interest.

■ ACKNOWLEDGMENTS

We appreciate the support from the National Natural Science Foundation of China (U1462119, 21506156, and U1463205), and the Tianjin Municipal Natural Science Foundation (15JCZDJC37300).

■ REFERENCES

(1) (a) Jiao, Y.; Zheng, Y.; Jaroniec, M.; Qiao, S. Z. *Chem. Soc. Rev.* **2015**, *44*, 2060. (b) Huang, Z.-F.; Song, J.; Pan, L.; Zhang, X.; Wang, L.; Zou, J.-J. *Adv. Mater.* **2015**, *27*, 5309. (c) Wang, S.; Pan, L.; Song, J.; Mi, W.; Zou, J. J.; Wang, L.; Zhang, X. *J. Am. Chem. Soc.* **2015**, *137*, 2975. (d) Huang, Z.-F.; Song, J.; Pan, L.; Wang, Z.; Zhang, X.; Zou, J.-J.; Mi, W.; Zhang, X.; Wang, L. *Nano Energy* **2015**, *12*, 646. (e) Berglund, S. P.; He, H.; Chemelewski, W. D.; Celio, H.; Dolocan, A.; Mullins, C. B. *J. Am. Chem. Soc.* **2014**, *136*, 1535. (f) Fei, H.; Dong, J.; Arellano-Jimenez, M. J.; Ye, G.; Dong Kim, N.; Samuel, E. L.; Peng, Z.; Zhu, Z.; Qin, F.; Bao, J.; Yacaman, M. J.; Ajayan, P. M.; Chen, D.; Tour, J. M. *Nat. Commun.* **2015**, *6*, 8668. (g) Tavakkoli, M.; Kallio, T.; Reynaud, O.; Nasibulin, A. G.; Johans, C.; Sainio, J.; Jiang, H.; Kauppinen, E. I.; Laasonen, K. *Angew. Chem., Int. Ed.* **2015**, *54*, 4535. (h) Xie, G.; Zhang, K.; Guo, B.; Liu, Q.; Fang, L.; Gong, J. R. *Adv. Mater.* **2013**, *25*, 3820. (i) Zhang, K.; Liu, Q.; Wang, H.; Zhang, R.; Wu, C.; Gong, J. R. *Small* **2013**, *9*, 2452.

(2) (a) Morales-Guio, C. G.; Stern, L.-A.; Hu, X. *Chem. Soc. Rev.* **2014**, *43*, 6555. (b) Xie, J.; Zhang, J.; Li, S.; Grote, F.; Zhang, X.; Zhang, H.; Wang, R.; Lei, Y.; Pan, B.; Xie, Y. *J. Am. Chem. Soc.* **2013**, *135*, 17881. (c) Gao, M. R.; Liang, J. X.; Zheng, Y. R.; Xu, Y. F.; Jiang, J.; Gao, Q.; Li, J.; Yu, S. H. *Nat. Commun.* **2015**, *6*, 5982. (d) Voiry, D.; Yamaguchi, H.; Li, J.; Silva, R.; Alves, D. C.; Fujita, T.; Chen, M.; Asefa, T.; Shenoy, V. B.; Eda, G.; Chhowalla, M. *Nat. Mater.* **2013**, *12*, 850. (e) Chen, Z.; Cummins, D.; Reinecke, B. N.; Clark, E.; Sunkara, M. K.; Jaramillo, T. F. *Nano Lett.* **2011**, *11*, 4168. (f) Yang, J.; Voiry, D.; Ahn, S. J.; Kang, D.; Kim, A. Y.; Chhowalla, M.; Shin, H. S. *Angew. Chem., Int. Ed.* **2013**, *52*, 13751. (g) Long, X.; Li, G.; Wang, Z.; Zhu,

DOI: 10.1021/jacs.5b11986
J. Am. Chem. Soc. 2016, 138, 1359–1365

H.; Zhang, T.; Xiao, S.; Guo, W.; Yang, S. *J. Am. Chem. Soc.* **2015**, *137*, 11900.
(3) (a) Bishop, P. E.; Premakumar, R.; Dean, D. R.; Jacobson, M. R.; Chisnell, J. R.; Rizzo, T. M.; Kopczynski, J. *Science* **1986**, *232*, 92. (b) Chan, M. K.; Kim, J.; Rees, D. *Science* **1993**, *260*, 792. (c) Volbeda, A.; Charon, M.-H.; Piras, C.; Hatchikian, E. C.; Frey, M.; Fontecilla-Camps, J. C. *Nature* **1995**, *373*, 580. (d) Brown, K. A.; Wilker, M. B.; Boehm, M.; Dukovic, G.; King, P. W. *J. Am. Chem. Soc.* **2012**, *134*, 5627.
(4) (a) Zou, X.; Huang, X.; Goswami, A.; Silva, R.; Sathe, B. R.; Mikmekova, E.; Asefa, T. *Angew. Chem., Int. Ed.* **2014**, *53*, 4372. (b) Sun, Y.; Liu, C.; Grauer, D. C.; Yano, J.; Long, J. R.; Yang, P.; Chang, C. J. *J. Am. Chem. Soc.* **2013**, *135*, 17699. (c) Cao, B.; Veith, G. M.; Neuefeind, J. C.; Adzic, R. R.; Khalifah, P. G. *J. Am. Chem. Soc.* **2013**, *135*, 19186. (d) Faber, M. S.; Dziedzic, R.; Lukowski, M. A.; Kaiser, N. S.; Ding, Q.; Jin, S. *J. Am. Chem. Soc.* **2014**, *136*, 10053.
(5) (a) Srivastava, B. B.; Jana, S.; Pradhan, N. *J. Am. Chem. Soc.* **2011**, *133*, 1007. (b) Zhang, J.; Yu, J.; Zhang, Y.; Li, Q.; Gong, J. R. *Nano Lett.* **2011**, *11*, 4774. (c) Zhang, J.; Yu, J.; Jaroniec, M.; Gong, J. R. *Nano Lett.* **2012**, *12*, 4584. (d) Peng, Z.; Jia, D.; Al-Enizi, A. M.; Elzatahry, A. A.; Zheng, G. *Adv. Energy Mater.* **2015**, *5*, n/a.
(6) (a) Staszak-Jirkovsky, J.; Malliakas, C. D.; Lopes, P. P.; Danilovic, N.; Kota, S. S.; Chang, K.-C.; Genorio, B.; Strmcnik, D.; Stamenkovic, V. R.; Kanatzidis, M. G.; Markovic, N. M. *Nat. Mater.* **2016**, *15*, 197. (b) Miao, J.; Xiao, F.-X.; Yang, H. B.; Khoo, S. Y.; Chen, J.; Fan, Z.; Hsu, Y.-Y.; Chen, H. M.; Zhang, H.; Liu, B. *Sci. Adv.* **2015**, *1*, e1500259.
(7) (a) An, K.; Kwon, S. G.; Park, M.; Na, H. B.; Baik, S.-I.; Yu, J. H.; Kim, D.; Son, J. S.; Kim, Y. W.; Song, I. C.; Moon, W. K.; Park, H. M.; Hyeon, T. *Nano Lett.* **2008**, *8*, 4252. (b) Wu, H. B.; Xia, B. Y.; Yu, L.; Yu, X.-Y.; Lou, X. W. *Nat. Commun.* **2015**, *6*, 6512. (c) Liu, H.; Joo, J. B.; Dahl, M.; Fu, L.; Zeng, Z.; Yin, Y. *Energy Environ. Sci.* **2015**, *8*, 286. (d) Martin, D. J.; Qiu, K.; Shevlin, S. A.; Handoko, A. D.; Chen, X.; Guo, Z.; Tang, J. *Angew. Chem., Int. Ed.* **2014**, *53*, 9240. (e) Yin, Y.; Rioux, R. M.; Erdonmez, C. K.; Hughes, S.; Somorjai, G. A.; Alivisatos, A. P. *Science* **2004**, *304*, 711.
(8) (a) Huang, Z.-F.; Song, J.; Pan, L.; Lv, F.; Wang, Q.; Zou, J.-J.; Zhang, X.; Wang, L. *Chem. Commun.* **2014**, *50*, 10959. (b) Lou, X. W.; Archer, L. A.; Yang, Z. *Adv. Mater.* **2008**, *20*, 3987.
(9) (a) Wu, R.; Qian, X.; Rui, X.; Liu, H.; Yadian, B.; Zhou, K.; Wei, J.; Yan, Q.; Feng, X. Q.; Long, Y.; Wang, L.; Huang, Y. *Small* **2014**, *10*, 1932. (b) Tang, J.; Salunkhe, R. R.; Liu, J.; Torad, N. L.; Imura, M.; Furukawa, S.; Yamauchi, Y. *J. Am. Chem. Soc.* **2015**, *137*, 1572. (c) Wu, R.; Wang, D. P.; Rui, X.; Liu, B.; Zhou, K.; Law, A. W.; Yan, Q.; Wei, J.; Chen, Z. *Adv. Mater.* **2015**, *27*, 3038. (d) Wu, R.; Qian, X.; Zhou, K.; Wei, J.; Lou, J.; Ajayan, P. M. *ACS Nano* **2014**, *8*, 6297. (e) Chen, Y.-Z.; Wang, C.; Wu, Z.-Y.; Xiong, Y.; Xu, Q.; Yu, S.-H.; Jiang, H.-L. *Adv. Mater.* **2015**, *27*, 5010.
(10) (a) Kresse, G.; Hafner. *Phys. Rev. B: Condens. Matter Mater. Phys.* **1993**, *47*, 558. (b) Kresse, G.; Hafner, J. *Phys. Rev. B: Condens. Matter Mater. Phys.* **1994**, *49*, 14251. (c) Perdew, J. P.; Burke, K.; Ernzerhof, M. *Phys. Rev. Lett.* **1996**, *77*, 3865. (d) Kresse, G.; Joubert, D. *Phys. Rev. B: Condens. Matter Mater. Phys.* **1999**, *59*, 1758.
(11) (a) Arai, T.; Senda, S.-i.; Sato, Y.; Takahashi, H.; Shinoda, K.; Jeyadevan, B.; Tohji, K. *Chem. Mater.* **2008**, *20*, 1997. (b) Li, J.; Wang, Y.; Zhou, T.; Zhang, H.; Sun, X.; Tang, J.; Zhang, L.; Al-Enizi, A. M.; Yang, Z.; Zheng, G. *J. Am. Chem. Soc.* **2015**, *137*, 14305. (c) Li, H.; Tsai, C.; Koh, A. L.; Cai, L.; Contryman, A. W.; Fragapane, A. H.; Zhao, J.; Han, H. S.; Manoharan, H. C.; Abild-Pedersen, F.; Norskov, J. K.; Zheng, X. *Nat. Mater.* **2015**, *15*, 48.
(12) (a) Deng, J.; Ren, P.; Deng, D.; Bao, X. *Angew. Chem., Int. Ed.* **2015**, *54*, 2100. (b) Nørskov, J. K.; Bligaard, T.; Logadottir, A.; Kitchin, J. R.; Chen, J. G.; Pandelov, S.; Stimming, U. *J. Electrochem. Soc.* **2005**, *152*, J23. (c) Greeley, J.; Jaramillo, T. F.; Bonde, J.; Chorkendorff, I. B.; Norskov, J. K. *Nat. Mater.* **2006**, *5*, 909.
(13) (a) Subbaraman, R.; Tripkovic, D.; Strmcnik, D.; Chang, K.-C.; Uchimura, M.; Paulikas, A. P.; Stamenkovic, V.; Markovic, N. M. *Science* **2011**, *334*, 1256. (b) Yin, H.; Zhao, S.; Zhao, K.; Muqsit, A.; Tang, H.; Chang, L.; Zhao, H.; Gao, Y.; Tang, Z. *Nat. Commun.* **2015**, *6*, 6430. (c) Weng, Z.; Liu, W.; Yin, L. C.; Fang, R.; Li, M.; Altman, E. I.; Fan, Q.; Li, F.; Cheng, H. M.; Wang, H. *Nano Lett.* **2015**, *15*, 7704.

DOI: 10.1021/jacs.5b11986
J. Am. Chem. Soc. 2016, 138, 1359−1365